1993A&A...273..160W

Astron. Astrophys. 273, 160–168 (1993)

ASTRONOMY AND ASTROPHYSICS

Period and disk radius changes in the dwarf nova IP Pegasi*

S. Wolf[2], K.H. Mantel[2], K. Horne[1], H. Barwig[2], R. Schoembs[2], and O. Baernbantner[2]

[1] Space Telescope Science Institute, 3700 San Martin Drive, Baltimore, MD 21218, USA
[2] Universitäts-Sternwarte, Scheinerstrasse 1, W-8000 München 80, Germany

Received November 12, 1992; accepted February 6, 1993

Abstract. We present UBVRI observations of 49 eclipses of the dwarf nova IP Peg obtained during a long term observing campaign between July 1990 and December 1991. We combine these data with previously published ones in order to study long term period variations and to measure changes in disk radius associated with the dwarf nova outbursts. Analysis of white dwarf egress timings from 1984-1991 shows that the 3.8 h orbital period varies sinusoidally with a period of 4.7 years. This change can be explained by a third body (late M dwarf) with a most probable mass of 0.10 $M_\odot$. Attempts to explain the change in period by magnetic activity on the secondary star fail, because the required variation in luminosity of the secondary is not observed. From measurements of hot spot ingress and egress timings we determine a mass ratio $q = M_2/M_1$ of 0.6 and a steadily decreasing disk radius during decline from outburst.

Key words: stars: binaries: eclipsing – novae, cataclysmic variables – stars: individual: IP Peg

1. Introduction

Cataclysmic Variables (CVs) are semi-detached close binary systems which consist of a white dwarf (primary) and a Roche-lobe-filling main sequence star (secondary). Matter is transfered from the inner Lagrangian point via an accretion disk onto the white dwarf. At the outer rim of the accretion disk where the mass stream hits the disk a hot spot is produced. In dwarf novae, an instability modulates either the rate of mass injection from the red star to the disk, or the rate of mass transfer through the disk, producing changes in the disk's luminosity and structure. Studies of eclipsing dwarf novae allows us to measure disk structure changes associated with the outbursts and hence to test rival theories and disk instability models.

The eclipsing dwarf nova IP Peg exhibits a typical quiescent accretion disk spectrum with strong double-peaked Balmer emission line profiles (Marsh 1988) indicating emissivities scaling with radius as $R^{-3/2}$. Infrared photometry reveals ellipsoidal variations from the secondary star (Szkody & Mateo 1986), and its radial velocity curve has been measured (Martin et al. 1989). The orbital light curve (Wood & Crawford 1986) shows a remarkably strong orbital hump and eclipse features of the hot spot and white dwarf, which will serve us here as diagnostics for the determination of period changes.

IP Peg's 3.8 h orbital period is the longest of the handful of known deeply-eclipsing dwarf novae, and the only one above the 2-3 h period gap. In several short-period eclipsing dwarf novae, e.g. OY Car, Z Cha, HT Cas, very precise system parameters have been measured using hot spot and white dwarf eclipse timings. Attempts to do the same for IP Peg have been hampered because the white dwarf ingress is blended with that of the hot spot. The white dwarf egress feature is visible, but it appears to be less stable than in the short-period systems so far studied. Nevertheless there is quite good agreement in the system parameters deduced photometrically (Wood & Crawford 1986; Wood et al. 1989) and from spectroscopy (Marsh 1988; Martin et al. 1989; Hessman 1989).

Wood et al. (1989) discussed the eclipse timings gathered in 1986-88. The orbital period was found to be increasing rapidly, with $P/\dot{P} = 4 \times 10^5$yr. The cause of such rapid period changes was unclear. Possible explanations include a third body in the system, or changes in radius of the secondary star possibly due to magnetic activity. Hot spot eclipse timings were used to track the disk radius as it decreased by over 20 percent in the quiescent period following two outbursts. The disk radius expands as angular momentum is carried outward by the viscosity during outburst, then shrinks again as low angular momentum material is added by the gas stream in quiescence. Analysis of this effect indicated that at least $7 \times 10^{-11} M_\odot$ is left in the outer disk following the eruption (Anderson 1988). More intensive monitoring of the mass injection rate and of disk radius changes over several outbursts offers the prospect of measuring the viscosity in quiescence.

In this paper we discuss results obtained between July 1990 and December 1991 from a campaign to monitor the eclipses of IP Peg with the 3-star UBVRI photometer (MCCP) on the

Send offprint requests to: S. Wolf

* Based on observations collected at the Mt. Wendelstein Observatory, Germany

© European Southern Observatory • Provided by the NASA Astrophysics Data System

1993A&A...273..160W

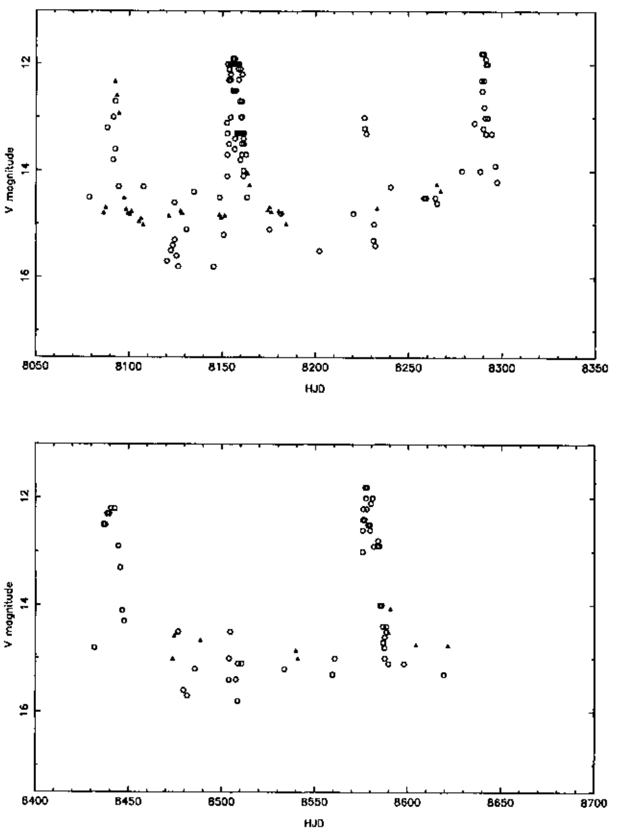

Fig. 1. Observations of IP Peg in the V filter published by the American Association of Variable Star Observers (AAVSO) signed by circles. Mean fluxes of observations presented in this paper are marked by filled triangles

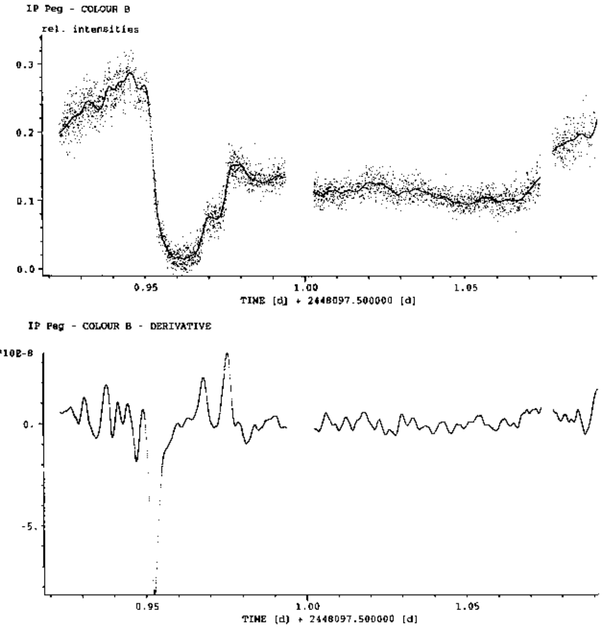

Fig. 2. The upper panel shows a B light curve together with a spline fit. From the spline fit the derivative presented in the lower panel was calculated. The ingress and egress timings of the hot spot and the white dwarf, respectively, are identified with the sharp peaks

0.8 m telescope at Mt. Wendelstein Observatory. In Section 2, we discuss the observations. Section 3 presents an analysis of the eclipse timings of the white dwarf and discusses hot spot eclipse timings used to monitor disk radius changes during the decline from outburst and the following quiescence phase. Section 4 summarizes the results.

2. Observations

2.1. Data acquisition and calibration

The observations were performed with the 3-star-UBVRI photometer (MCCP) attached to the 0.8 m telescope at Mt. Wendelstein in the Bavarian Alps. This instrument has been designed to measure the object, a nearby comparison star, and the sky background simultaneously in 5 colours (UBVRI) with high time resolution (Barwig et al. 1987). The simultaneous measurements allow a nearly complete compensation for changing atmospheric extinction effects and varying background contributions. High precision, differential photometric measurements of IP Peg relative to a nearby comparison star were obtained, on 45 nights. A journal of the IP Peg observations is given in Table 1. On most nights, an integration time of 2 seconds was used, excluding one night in October 1991 and two nights in September 1990 where data were recorded with an intergration time of 1 and 4 seconds, respectively. Figure 1 shows our data together with the AAVSO light curve of IP Peg. In the course of the campaign, data on 43 eclipses in quiescence and 6 eclipses on the decline from two outbursts were recorded. All measurements were reduced relative to a nearby comparison star using standard reduction procedures (Barwig et al. 1987).

2.2. Ephemeris and period changes

Wood et al. (1989) found the orbital period of IP Peg to be increasing in 1986 to 1988 at a remarkably high rate of $P/\dot{P} = 4 \times 10^5$yr. The white dwarf egress is visible in many of our eclipses as a quick rise of the count rate at the expected phase 0.043, particularly in the B and V channels, often in U and R, but seldom in I. The white dwarf egress feature varies significantly in width and intensity from cycle to cycle. This may possibly be interpretable in terms of changing obscuration, or alternatively of a variable boundary layer component.

We measured the mid phase of the white dwarf egress by taking the derivative of the eclipse light curve in the B channel and measuring the phase of maximum slope (see Fig. 2). This measurement was done by an interpolating spline routine in order to improve its accuracy. The timings thereby obtained and listed in Table 2 extend by 4 years the 2-year baseline of the earlier timings reported by Wood et al. (1989). In Fig. 3 we show the O-C residuals for the white dwarf egress relative to the ephemeris

$$HJD = 2445615.4224(4) + 0.15820616(4) \cdot E \quad . \tag{1}$$

© European Southern Observatory • Provided by the NASA Astrophysics Data System

1993A&A...273..160W

Table 1. Journal of observations. (IT: integration time, $V_{0.25}$-flux: V-flux at phase 0.25)

date	HJD-start [−2440000.0]	obs.hours [h]	IT [s]	$<V_{0.25}$-flux$>$ [mag]	start cycle	end cycle
13-07-90	8086.473213	2.48	2	14.80087	15619.18	15619.84
14-07-90	8087.445635	3.36	2	14.70133	15625.33	15626.21
19-07-90	8092.431453	3.87	2	12.34009	15656.84	15657.86
20-07-90	8093.438276	3.55	2	12.59894	15663.21	15664.14
21-07-90	8094.410393	4.29	2	12.93119	15669.35	15670.48
22-07-90	8095.429332	1.36	2	–	15675.79	15676.15
24-07-90	8097.444252	3.44	2	14.51874	15688.53	15689.43
25-07-90	8098.417975	4.17	2	14.73685	15694.68	15695.78
26-07-90	8099.398818	2.54	2	14.80990	15700.88	15701.55
27-07-90	8100.410949	4.19	2	14.82021	15707.28	15708.38
28-07-90	8101.408242	4.23	2	14.76935	15713.58	15714.70
01-08-90	8105.391223	4.85	2	14.96048	15738.76	15740.04
02-08-90	8106.408740	4.49	2	14.90382	15745.19	15746.37
03-08-90	8107.396599	4.66	2	15.01875	15751.44	15752.66
17-08-90	8121.344535	5.52	2	14.85568	15839.60	15841.05
19-08-90	8123.347401	2.92	2	–	15852.26	15853.03
23-08-90	8127.315070	7.25	2	14.76227	15877.34	15879.25
24-08-90	8128.328293	6.99	2	14.80460	15883.74	15885.58
13-09-90	8148.292741	8.56	4	14.82563	16009.94	16012.19
14-09-90	8149.290598	7.31	4	14.88289	16016.24	16018.17
16-09-90	8151.301286	4.74	2	14.84624	16028.95	16030.20
28-09-90	8163.470010	2.40	2	14.05299	16105.87	16106.50
29-09-90	8164.463553	4.02	2	14.27527	16112.15	16113.21
09-10-90	8174.331048	6.56	2	14.74755	16174.52	16176.25
10-10-90	8175.263864	6.84	2	14.68790	16180.42	16182.22
11-10-90	8176.252403	6.57	2	14.77880	16186.66	16188.39
15-10-90	8180.274045	7.57	2	14.76409	16212.08	16214.08
16-10-90	8181.284664	5.95	2	–	16218.47	16220.04
17-10-90	8182.326416	2.46	2	14.78786	16225.06	16225.70
19-10-90	8184.295041	4.35	2	15.00161	16237.50	16238.65
07-12-90	8233.233903	4.68	2	14.70609	16546.84	16548.07
08-01-91	8265.225102	2.78	2	14.25167	16749.05	16749.78
10-01-91	8267.218626	3.09	2	14.37329	16761.65	16762.46
04-08-91	8473.366493	5.60	2	15.01794	18064.68	18066.16
05-08-91	8474.350579	5.95	2	14.58715	18070.90	18072.47
06-08-91	8475.425789	4.24	2	14.53704	18077.70	18078.82
19-08-91	8488.444551	3.92	2	14.66530	18159.99	18161.02
09-10-91	8539.328403	6.56	1	14.85525	18481.62	18483.35
10-10-91	8540.254307	9.28	2	15.01299	18487.47	18489.92
11-10-91	8541.253177	1.38	2	–	18493.79	18494.15
28-11-91	8589.204605	5.17	2	14.52291	18796.87	18798.24
29-11-91	8590.201613	5.81	2	14.07684	18803.18	18804.71
12-12-91	8603.212014	5.69	2	–	18885.42	18886.92
13-12-91	8604.187895	6.29	2	14.75174	18891.59	18893.24
30-12-91	8621.336407	1.55	2	14.76645	18999.98	19000.39

IP Peg clearly no longer follows the quadratic ephemeris established by Wood et al. (1989) from the 1986-88 timings. The O-C residuals to date can be fitted by the sine curve,

$$O - C = A_3 \cdot \sin(2\pi \cdot [E - E_3]/P_3) \quad , \tag{2}$$

with a period $P_3 = 4.7 \pm 0.2$ years, epoch $E_3 = 10258 \pm 130$ and semi amplitude $A_3 = 1.57 \pm 0.14$ minutes.

2.3. Mass ratio and disk radius variations

The hot spot located on the outer rim of the accretion disk is caused by the impact of the gas stream from the secondary star. Because the ballistic trajectory of the stream is determined only by the mass ratio of the binary, we can use hot spot eclipse timings to locate the spot along the stream trajectory and thereby to determine the binary mass ratio q and the radius of the accretion disk. Wood et al. (1989) used this method to estimate

© European Southern Observatory • Provided by the NASA Astrophysics Data System

1993A&A...273..160W

Table 2. White dwarf egress-timings t_{we} and hot spot ingress- and egress phases (ϕ_{hi}, ϕ_{he}) determined from the maximum of the derivative of the eclipse light curve in the B channel. These phases were used to calculate the disk radius R_d. The ephemeris given in Eq. (1) was used to determine the cycle number and the phases. Values of low quality are set in brackets

date	cycle	t_{we} $[HJD - 2440000.0]$	ϕ_{hi}	ϕ_{he}	R_d $[a]$
90-07-14	15626	(8087.55316)	-0.041	+0.082	0.2405420
90-07-19	15657	–	–	+0.095	–
90-07-20	15664	–	-0.060	+0.103	0.3731107
90-07-21	15670	–	-0.059	+0.095	0.3440684
90-07-24	15689	8097.51853	-0.055	+0.094	0.3304576
90-07-25	15695	8098.46710	-0.055	+0.093	0.3266707
90-07-26	15701	(8099.41700)	-0.052	–	–
90-07-27	15708	8100.52467	-0.050	+0.093	0.3140995
90-07-28	15714	8101.47378	-0.054	+0.092	0.3202592
90-08-01	15739	–	-0.049	+0.092	0.2937009
90-08-02	15746	8106.53638	-0.046	+0.092	0.3001048
90-08-03	15752	(8107.48621)	-0.049	+0.091	0.3033649
90-08-17	15840	(8121.41476)	-0.045	+0.088	0.2800383
	15841	(8121.56578)	–	–	–
90-08-19	15853	–	-0.042	–	–
90-08-23	15878	8127.41936	-0.048	+0.088	0.2879603
	15879	8127.57776	-0.042	+0.088	0.2723677
90-08-24	15884	(8128.36905)	-0.043	+0.086	0.2702921
	15885	(8128.52494)	(-0.038)	(+0.093)	(0.2861148)
90-09-13	16010	8148.30278	–	–	–
	16011	8148.46167	-0.041	+0.086	0.2604007
	16012	8148.61905	–	–	–
90-09-14	16017	8149.41041	-0.038	+0.089	0.2651599
	16018	8149.56844	-0.054	+0.088	0.2629890
90-09-16	16029	8151.30803	–	+0.092	–
	16030	8151.46720	-0.044	+0.091	0.2973005
90-09-28	16106	–	-0.058	+0.094	0.3379914
90-09-29	16113	–	–	+0.095	–
90-10-09	16175	(8174.40680)	-0.046	+0.092	0.3001049
	16176	(8174.56473)	(-0.054)	(+0.089)	(0.3084277)
90-10-10	16181	8175.35589	-0.047	+0.092	0.3025525
	16182	(8175.51461)	-0.049	+0.090	0.2991697
90-10-11	16187	8176.30523	-0.047	+0.090	0.2940087
	16188	8176.46336	-0.048	+0.091	0.3008220
90-10-15	16213	8180.41910	-0.047	+0.087	0.2808659
	16214	(8180.57656)	(-0.044)	(+0.092)	(0.2952924)
90-10-16	16219	–	-0.048	–	–
90-10-19	16238	–	-0.050	+0.089	0.2975968
90-12-07	16547	(8233.25941)	-0.048	+0.094	0.3133062
	16548	(8233.41869)	-0.052	+0.092	0.3151166
91-01-10	16762	–	-0.044	+0.090	0.2864674
91-08-04	18065	–	-0.046	+0.091	0.2958072
	18066	–	-0.048	–	–
91-08-05	18071	8474.36398	-0.050	–	–
	18072	8474.52361	-0.060	+0.084	0.3059864
91-08-06	18078	8475.47267	-0.046	+0.084	0.2781737
91-08-19	18160	–	–	+0.088	–
	18161	8488.60368	-0.052	–	–
91-10-09	18482	8539.38748	-0.039	+0.086	0.2529696
	18483	8539.54593	-0.038	+0.084	0.2429000
91-10-10	18488	8540.33718	-0.041	+0.083	0.2455945
	18489	8540.49555	-0.041	+0.084	0.2455946
91-10-11	18494	8541.28622	-0.039	+0.079	0.2453998
91-11-28	18797	8589.22210	-0.050	+0.093	0.3140995
	18798	8589.38048	-0.051	+0.093	0.3165843
91-11-29	18804	8590.33006	-0.047	+0.095	0.3150530

© European Southern Observatory • Provided by the NASA Astrophysics Data System

1993A&A...273..160W

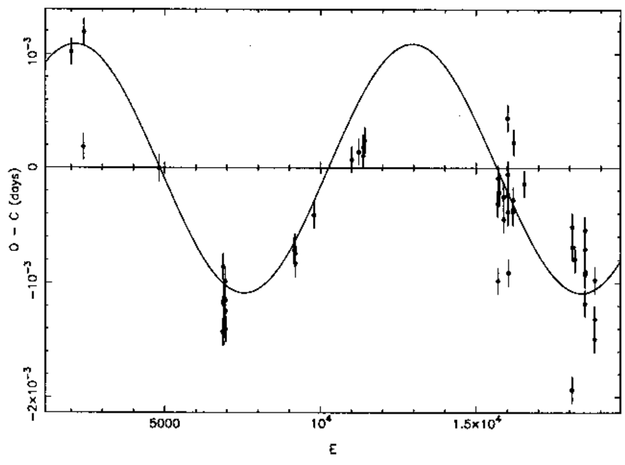

Fig. 3. O-C residuals calculated from the ephemeris given in equation (1) versus the cycle number E. A sine-fit according to equation (2) has been applied to the data. Data in the range of $2010 < E < 11428$ are taken from Wood et al. (1989)

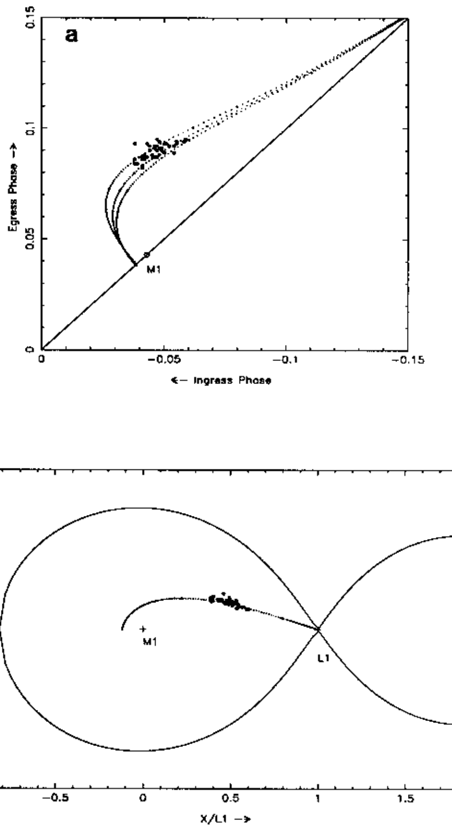

Fig. 4. a (upper panel) The ingress and egress phases of the hot spot, determined from hot spot eclipse timings (Table 2) and the eclipse width of the white dwarf $\Delta\phi_w = 0.086$ (Wood et al. 1989). Three different stream trajectories for mass ratios of $q = 0.4$, $q = 0.6$ and $q = 0.8$ are shown (left to right). **b** (lower panel) Projection of the hot spot ingress and egress phases onto the orbital plane, shown for a mass ratio of $q = 0.6$. Crosses mark the positions of the primary and secondary, respectively. Units are in distance between the white dwarf and the inner Lagrangian Point L_1 (= 0.55 a for $q = 0.6$)

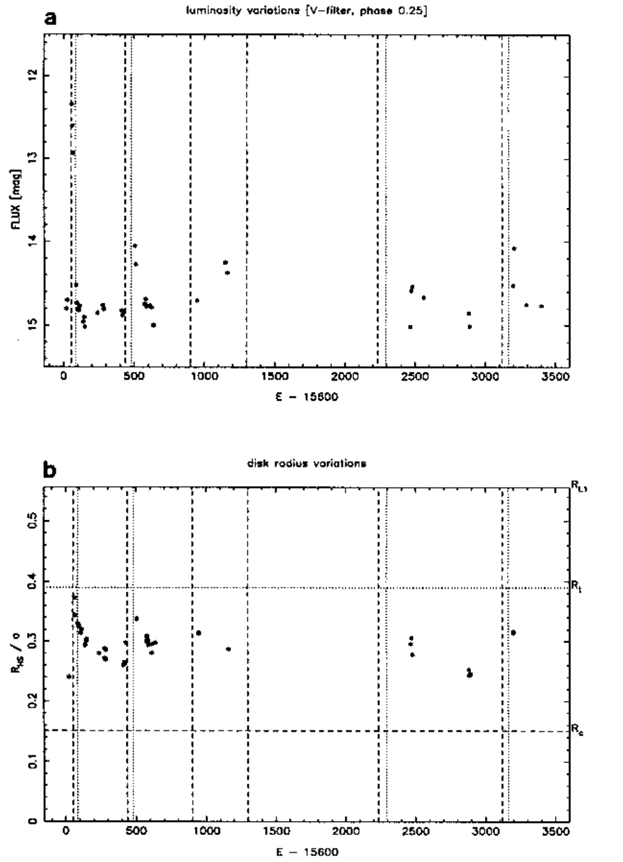

Fig. 5. a (upper panel) Luminosity variations as a function of time. The luminosity $V_{0.25}$ is an average of the V band over the phase interval 0.2 to 0.3 (see also Table 1). **b** (lower panel) Disk radii determined from the ingress and egress phases of the hot spot ϕ_{hi} and ϕ_{he} as a function of time. The dashed and dotted lines indicate the beginning and the end of an outburst. R_c is the radius of the circular orbit with the same specific angular momentum as material at the inner Lagrangian point (L_1). R_t is the tidal disk radius for a mass ratio of 0.6

$q = 0.49$ for IP Peg, and to show that significant changes in the disk radius occur in the quiescent periods between the dwarf nova outbursts.

The hot spot ingress and egress features are clearly visible in all of our light curves except for a few obtained on the decline from outburst. The hot spot egress is relatively easy to measure because it is a rather well defined rise in flux near the end of the eclipse. The ingress, however, is particularly difficult to measure because of its marked asymmetry. The initial rapid drop in brightness evolving into a more gradual decline indicates that the hot spot region has a bright head forming where the gas stream hits the disk, and a tail of cooling gas extending around the outer rim of the disk. The hot spot ingress is confused with the ingress of the white dwarf, but the white dwarf flux, as judged by its egress, is generally small enough not to significantly affect the hot spot timings. We found it useful to plot the time derivative of the light curve, which usually showed a sharp peak corresponding to the phase of most rapid decline in the hot spot flux, and it is this feature which we have measured

© European Southern Observatory • Provided by the NASA Astrophysics Data System

1993A&A...273..160W

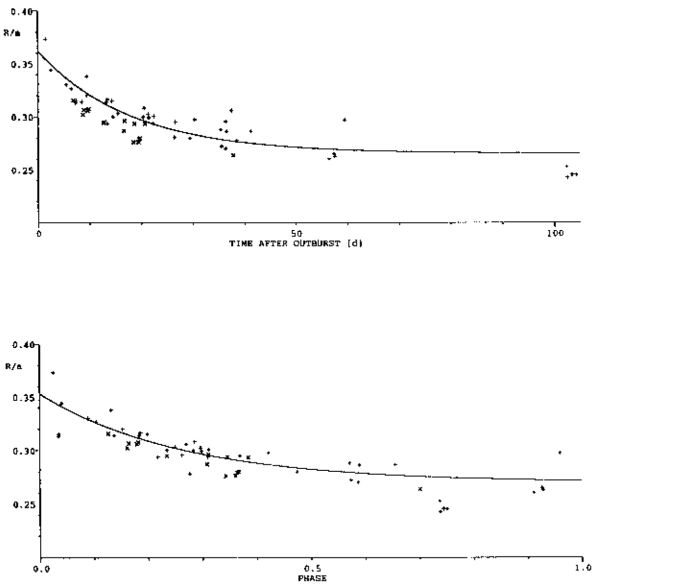

Fig. 6. Disk radius variation plotted as a function of time (upper panel) and a function of outburst phase (lower panel). An exponential function has been fitted to the data (solid line). Data of this paper are marked by '+', whereas data of Wood et al. (1989) are marked by '×'

(see Fig. 2). Our measurements of hot spot ingress and egress are collected in Table 2. The estimated accuracy of the timings varies between 10 s and 30 s.

Figure 4a shows the hot spot eclipse timings with predicted timings for locations along the gas stream trajectory for binary mass ratios of 0.4, 0.6, and 0.8, respectively. The white dwarf eclipse width was taken to be $\Delta\phi$ = 0.086 (Wood et al. 1989). The timings are compatible with a mass ratio of 0.6, close to the spectroscopic value 0.58 $\pm$ 0.06 (Marsh 1988), and a bit larger than the previous photometric value 0.49 (Wood and Crawford 1986, Wood et al. 1989). The cluster of observed hot spot timings is clearly extended in the direction of the gas stream with a mass ratio of q = 0.6, indicating that significant variations in the accretion disk radius occur. Figure 4b projects the hot spot timings onto the plane of the accretion disk, showing explicitly the range of variations in the disk radius.

The disk radius as a function of time is shown in Fig. 5b. Just prior to the first outburst observed in the campaign, the disk radius was quite small (0.24 a) although larger than the minimum radius (R_c = 0.1058 a for q = 0.6, Lubow & Shu 1975), where a ring of material would build up if the specific angular momentum of the material from the L1 point were to remain constant rather than being redistributed by viscosity. However, the observed radius is much smaller than the tidal disk radius, R_t = 0.39 a for q = 0.6, where tidal torques efficiently extract angular momentum from the disk (Paczinsky 1977). The disk radius was next observed to be 0.37 a on the decline from the first outburst, nearly twice its pre-outburst radius. This expanded disk then declines toward what appears to be a new equilibrium radius at 0.26 a. The second outburst was observed less completely than the first. The disk was found to be expanded to 0.34 a on the decline, but it was back down to 0.28 a several days later. During the following outburst cycles, only a few observations were made; unfortunately no complete decline from outburst is seen.

In order to compare the rate of shrinking during different ouburst cycles, we plot in Fig. 6 the disk radius as a function of time elapsed after outburst and as a function of outburst phase respectively. If t_p and t_f are the times of the preceeding and the following outburst, then the outburst phase at time t is given by $(t - t_p)/(t_f - t_p)$. In order to compare results of this campaign with the former findings of Wood et al. (1989), their data have also been added to Fig. 6. Because they used a q-value of 0.49, new disk radii based on a q-value of 0.6 were computed from their hot spot eclipse timings. Although disk radii from 6 different outburst cycles over a time range of 5 years have been combined in Fig. 6, good agreement in the rate of shrinkage is found. The decline is consistent with an exponential decay in the disk radius for both diagrams, with a decay constant of 0.06 d^{-1} and an equilibrium radius of 0.27 a in the radius versus time after outburst plot. This decay constant corresponds to a half-life-time of 11.55 d. The exponential fit in the radius versus outburst phase plot predicts the same equilibrium radius and a decay constant of 3.8. From the observations obtained so far we cannot decide whether the disk radius is more closely related with the time elapsed after an outburst or with outburst phase.

The disk radius variations observed for IP Peg are similar to those seen in observations of U Gem (Smak 1984) and Z Cha (O'Donoghue 1986). Both systems show a rapid decline in disk radius shortly after an outburst and a longterm decrease on a smaller scale during the following quiescence phase. O'Donoghue notes that an exponential decline gives a poor fit to his data because he found a rapid disk radius decrease just before an outburst. Smak states that the disk variations in U Gem can be described by an exponential shrinkage between two outbursts with a decay constant of 0.07 d^{-1} – this is in good agreement with our result.

In Fig. 5a the luminosity variations in the V band at phase 0.25 is shown. The first two outburst cycles were nearly completly recorded and show a rapid increase and a sudden decrease in luminosity reaching a constant value until the next outburst starts. Ichikawa & Osaki (1992) compared the disk instability model (DIM) and the mass transfer model (MTM) concerning their predictions for luminosity and disk radius variations. They showed that the MTM leads to a slow decrease in luminosity on the same time scale as the disk radius. In contrast to this the DIM just shows a luminosity peak for several days and a rapid drop to a constant value while the radius shrinks throughout the whole outburst cycle. According to these results and our observations the DIM is the preferred model in explaining the outburst mechanism for dwarf novae.

© European Southern Observatory • Provided by the NASA Astrophysics Data System

1993A&A...273..166W

3. Discussion

3.1. Magnetic activity cycles

Period changes on timescales of years have also been found in other cataclysmic variables (e.g. UX UMa, RW Tri, U Gem, DQ Her, T Aur, EX Hya, Z Cha, see Warner 1988) and there have been attempts to explain the period variations in terms of cycles of magnetic activity on the secondary star (Matese and Whitmire 1983, Van Buren and Young 1985, Applegate and Patterson 1987, Warner 1988). These authors proposed that a changing magnetic field deforms the secondary, distorting it away from a fluid equilibrium shape. However, these models were dealt a serious blow by Marsh and Pringle (1990), who found that the amount of energy required to distort the secondary and to keep it in the new non-equilibrium state was larger than the luminosity the star could provide. Applegate (1992) proposed a new model where the changing magnetic field triggers transitions between different fluid hydrostatic equilibria. In contrast to the former models, smaller magnetic fields and much less energy are needed. During these transitions the secondary will be deformed. These deformations can be described by the quadrupole moment of the rotating star, which depends on the distribution of the angular moment within the star. As the moment of inertia at the outer layers of the star is much higher than in the inner parts, the quadrupole moment will mainly be influenced by an outer shell of the secondary. Thus Applegate introduced such a shell at a radius R with a mass $M_S \approx 0.1 M_\odot$ and a moment of inertia $I_S = \frac{2}{3} M_S R^2$. The quadrupole moment Q increases when angular momentum J is transfered into the outer shell – $\Delta Q/\Delta J > 0$. Every change in the quadrupole moment changes the gravitational potential of the star which has to be balanced by an increasing or decreasing centrifugal acceleration (v^2/r). As a consequence of this balance and the conservation of angular momentum the orbital period will decrease or increase, respectively. If the energy ΔE required to transfer the angular momentum ΔJ is supplied by the nuclear luminosity of the star without any energy storage in the convective zone, the star should show luminosity variations of the order of $\Delta E/P_{mod}$, where P_{mod} is the period of the orbital period modulation. The calculated energy variation need not appear completely as a luminosity variation, especially, if the angular momentum exchange occurs between the convective envelope and the inner radiative part of the star. The dissipated rotational energy in the radiative zone will not contribute to the luminosity variation because radiative zones cannot respond faster than the local Kelvin-Helmoltz time which is much longer than the modulation period P_{mod}.

Taking the values for $R_2 = 0.491 R_\odot$, $M_2 = 0.64 M_\odot$, $a = 1.47 R_\odot$, $P = 0.15820616$ d from Marsh (1988) and the values of $A_3 = 1.57$ min and $P_3 = 4.7$ years from our sine-fit Eq. (2), a change in angular momentum $\Delta J = -8 \times 10^{46}$erg s and a magnetic field strength of 5×10^5G can be computed from Applegate's equations (27) and (33). This value exceeds by two orders of magnitude the 10^3 G magnetic field strengths expected at the surfaces of main sequence stars. Together with the standard assumptions that the mass in the outer shell of the secondary M_S amounts to 0.1 M_2 and that the transfer of ΔJ to the outer shell will spin up the shell by an angular velocity $\Delta\Omega = 0.047\ d^{-1}$ a change in energy $\Delta E = 1.1 \times 10^{41}$erg could be derived (equation (28), Applegate 1992). This change in energy is related to a change in luminosity of $\Delta L = 0.612 L_\odot$. Assuming that the secondary lies close to the main sequence (Marsh, 1988) the luminosity of the secondary of $L_2 = 0.22 L_\odot$ can be estimated from the mass-luminosity function for the main sequence. Therefore according to the model proposed by Applegate (1992), the secondary star should undergo a change in luminosity of about 300% during the 4.7 years magnetic cycle. In order to test this prediction we compared the level of the I-lightcurve during eclipse of the white dwarf and of the hot spot, which should represent a good measure for the luminosity of the secondary, at different times of the 4.7 years cycle. However, only erratic variations of the order of 5% are found. Assuming angular moment transfer between a convective envelope and an inner radiative part decreases the required energy by a factor of 3 to $\Delta E = 3.4 \times 10^{40}$ but the luminosity change $\Delta L = 0.19\ L_\odot$ remains too high to be found in our observations.

If magnetic activity is the underlying process for the observed changes in period, there should be correlations between orbital period changes and magnetic activity indicators e.g. varying chromospheric emission lines from the secondary. There have been extensive spectroscopic studies during the minimum and the outburst stage of IP Peg by Martin et al. (1987), Marsh (1988), Martin et al. (1989), Hessman (1989), Piché and Szkody (1989) and Marsh & Horne (1990) covering a time interval of about 2 years. During the quiescent phase no emission lines from the secondary could be detected. Narrow chromospheric emission lines from the secondary star could only be seen during decline from outburst and could be clearly attributed to irradiation from the boundary layer and the accretion disk (Martin et al. 1987). Therefore, the fact that no indications for magnetic activity could be found and the disproved change in luminosity of the secondary star, predicted by the model proposed by Applegate (1992), cast considerable doubt on magnetic activity as the underlying mechanism for the observed orbital period variations in IP Peg.

3.2. A third body in the system

We are left with a third body in the system to account for the period changes in IP Peg. If the binary, of mass $M_1 + M_2 = M$ ($M_1 = 1.09\ M_\odot$, $M_2 = 0.64\ M_\odot$) and a third body orbit around their common center of gravity with period P_3 in a plane which is inclined towards the observer, then the following equations may be derived from Kepler's law:

$$m_3^3 - \frac{G}{4\pi^2}\left(\frac{c\,A_3}{\sin(i_3)}\right)^3 \frac{(m_3+M)^2}{P_3^2} = 0 \qquad (3)$$

with m_3 mass of the third body, M mass of the binary and i_3 inclination between third body and binary, c the speed of light, G gravitational constant and A_3 the amplitude of the sine-fit to the time-delay curve.

© European Southern Observatory • Provided by the NASA Astrophysics Data System

1993A&A...273..160W

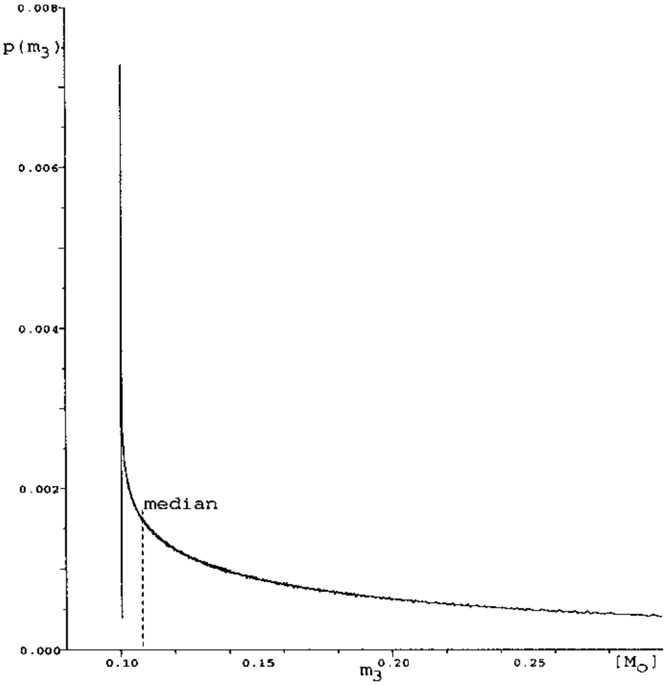

Fig. 7. Probability distribution for the mass of the third body

A probability distribution was used for the unknown inclination i_3, assuming a random orientation of the orbit. The probability function peaks at high inclination angles, because most of the solid angle is occupied by edge-on rather than pole-on orbits. Taking the value for M from Marsh (1988) and for A_3 and P_3 from the derived sine-fit (Eq.2) the mass probability distribution is computed as shown in Fig. 7. The minimum and most probable mass for the third body is 0.10 $M_\odot$, corresponding to a late M dwarf but not a brown dwarf or a planet; of course, much higher masses are possible depending on the value of i_3. The third star may then be expected to contribute to the near infrared spectra which have been used to measure the radial velocity curve of the secondary star (Marsh 1988). The observed value of K_2 and hence the masses could therefore be underestimated.

3.3. The accretion disk radius

The evolution of the disk radius is determined by a competition between two opposing influences: the gas stream injects low angular momentum material causing the disk to shrink, while viscosity transports angular momentum outward causing the disk to expand. The 'inertia' providing resistance to these opposing influences is proportional to the surface density of mass in the disk. These processes are discussed by Anderson (1988), who developed simple analytic models to illustrate the effects and to interpret the disk radius variations seen in U Gem and Z Cha. The rate of shrinking of the disk as it receives low angular momentum material from the gas stream can be used to place a lower limit on the mass in the disk – the disk shrinks faster if it holds less mass. This was first accomplished for IP Peg by Wood et al. (1989), who found that the quiescent disk must hold at least 0.7×10^{-10} $M_\odot$. The mass injection rate adopted for this estimate was 2.2×10^{-10} $M_\odot$/yr, as derived from analysis of the orbital hump and bright spot eclipses in quiescence.

According to Anderson (1988) a lower limit on the mass in the outer accretion disk M_d can be described by

$$M_d = \frac{1 - (R_c/R_{min})}{(R_{max}/R_{min}) - 1} \dot{M} \Delta t \quad , \qquad (4)$$

where R_{max} and R_{min} are the maximum and minimum observed disk radii, Δt is the time taken for the disk to shrink and R_c is the radius of the circular orbit with the same specific angular momentum as material at the inner Lagrangian point. Lubow and Shu (1975) calculated R_c as a function of mass ratio: for q = 0.6, R_c = 0.1058. Taking a mass transfer rate of 2.2×10^{-10} $M_\odot$ (Marsh 1988) we find a lower limit on the mass in the outer accretion disk of 0.9×10^{-10} $M_\odot$, which is close to the value found by Wood et al. (1989).

4. Conclusions

We have presented eclipse timings of 47 eclipses of IP Peg accumulated in 1990 and 1991. Analysis of white dwarf egress timings over a baseline of 6 years indicates a sinusoidal change in orbital period of IP Peg with a period of 4.7 years. Possible explanations include a third body with a minimum mass of 0.10 $M_\odot$ or magnetic activity on the secondary star. Magnetic activity would require an enormous luminosity change which is not observed. Future monitoring will be important to determine whether the system continues to follow a sinusoidal ephemeris. From hot spot eclipse timings a mass ratio of q = 0.6 is derived, in good agreement with the spectroscopic value of 0.58 found by Marsh (1988). The rate of shrinkage in disk radius during the decline from outburst is constant during different outburst cycles and can be fitted by an exponential function. This is in good agreement with disk radius variations observed in the dwarf nova U Gem. Simultaneous luminosity variations point to the disk instability model as an explanation for the outburst mechanism. From a simple outburst model a lower limit on the mass in the outer accretion disk of $9 \times 10^{-11} M_\odot$ is derived. We plan to estimate the mass injection rate as a function of time by modelling the UBVRI fluxes of the orbital hump and of the eclipses of the bright spot. We may then be able to combine the observed disk radius variations and mass injection rate histories to reconstruct the history of the radial distribution of mass and hence of angular momentum in the outer disk over the course of several outbursts.

Acknowledgements. We acknowledge the observations from the AAVSO international data base sent to us by AAVSO Director Janet A. Mattei. Keith Horne is grateful to the Universitäts-Sternwarte München for hospitality while the data were under analysis, and to the National Aeronautics and Space Administration for financial support through grants NAGW-2264 and NAGW-2678 to the Space Telescope Science Institute.

© European Southern Observatory • Provided by the NASA Astrophysics Data System

1993A&A...273..160W

References

Anderson, N., 1988, *Astrophys. J.*, **325**, 266.
Applegate, J.H. & Patterson, J., 1987, *Astrophys. J.*, **322**, L99.
Applegate, J.H., 1992, *Astrophys. J.*, **385**, 621.
Barwig, H., Schoembs, R., Buckenmayer, C., 1987, *Astr. Astrophys.* **175**, 327.
Hessman, F.V., 1989, *Astron. J.*, **98**, 675.
Ichikawa, S, Osaki, Y, 1992, *Publication of Astronomical Society of Japan*, **44**, 15.
Lubow, S.H., Shu, F.H., 1975, *Astrophys. J.*, **198**, 383.
Marsh, T.R., 1988, *Mon. Not. R. astr. Soc.*, **231**, 1117.
Marsh, T.R., Horne, K., 1990, *Astrophys. J.*, **349**, 593.
Marsh, T.R., Pringle, J.E., 1990, *Astrophys. J.*, **365**, 677.
Martin, J.S., Jones, D.H.P, Smith,R.C., 1987, *Mon. Not. R. astr. Soc.*, **224**, 1031.
Martin, J.S., Friend, M.T., Smith, R.C., Jones, D.H.P., 1989, *Mon. Not. R. astr. Soc.*, **240**, 519.
Matese, J.J., Whitmire, D.P., 1983, *Astr. Astrophys.*, **117**, L7.
Mattei, J.A., 1992, observations from the AAVSO international data base, private communication.
O'Donoghue, D., 1986, *Mon. Not. R. astr. Soc.*, **220**, 23p.
Paczynski, B., 1977, *Astrophys. J.*, **216**, 822.
Piché,F., Szkody,P., 1989, *Astron. J.*, **98**, 2225.
Smak, J., 1984, *Acta Astr.*, **34**, 161.
Szkody, P., Mateo, M., 1986, *Astron. J.*, **92**, 483.
Van Buren, D., Young, A., 1985, *Astrophys. J.*, **295**, L39.
Warner, B.W., 1988, *Nature*, **336**, 129.
Wood, J.H., Crawford, C.S., 1986, *Mon. Not. R. astr. Soc.*, **222**, 645.
Wood, J.H. Marsh, T.R., Robinson, E.L., Stiening, R.F., Horne, K., Stover, R.J., Schoembs, R., Allen, S.L., Bond, H.E., Jones, D.H.P., Grauer, A.D., Ciardullo, R., 1989, *Mon. Not. R. astr. Soc.*, **239**, 809.

This article was processed by the author using Springer-Verlag LaTeX A&A style file version 3.

© European Southern Observatory • Provided by the NASA Astrophysics Data System